

## Chemical composition and trajectories of atmospheric particles at the Machu Picchu Peruvian Antarctic scientific station (62.09° S, 58.47° W)

Daniel ÁLVAREZ-TOLENTINO<sup>1</sup>, Luis SUÁREZ-SALAS<sup>2</sup>,  
José POMALAYA-VALDEZ<sup>3\*</sup> and Boris BARJA<sup>4</sup>

<sup>1</sup> *Escuela Profesional de Ingeniería Ambiental, Universidad Nacional Intercultural de la Selva Central Juan Santos Atahualpa (UNISCJSA), Jirón Los Cedros 141, La Merced, Chanchamayo, Perú.*

<sup>2</sup> *Instituto Geofísico del Perú (IGP), Calle Badajoz 169, Ate, Lima, Perú.*

<sup>3</sup> *Facultad de Ingeniería Química, Universidad Nacional del Centro del Perú (UNCP), Av. Mariscal Castilla 3909, El Tambo, Huancayo, Perú.*

<sup>4</sup> *Departamento de Matemática y Física, Universidad de Magallanes, Av. Presidente Manuel Bulnes 01855, Punta Arenas, Chile.*

\*Corresponding author; email: [jpomalaya@uncp.edu.pe](mailto:jpomalaya@uncp.edu.pe)

Received: May 14, 2023; Accepted: February 6, 2024

### RESUMEN

La Antártida es una región remota, pero con importante influencia de las regiones circundantes. El transporte de aerosoles desde distancias lejanas es una importante fuente de contaminación que puede impactar esta región, especialmente la Península Antártica. Es necesario caracterizar los aerosoles atmosféricos y analizar la contribución de sus fuentes de emisión. Para ello se analizó durante febrero de 2020 la composición química elemental de las partículas atmosféricas PM<sub>10</sub> y PM<sub>2.5</sub>, y se realizaron mediciones de tanto de éstas como de carbono negro con análisis de retrotrayectoria de masas de aire utilizando el modelo HYSPLIT. El objetivo fue caracterizar los elementos traza, analizar las fuentes de material particulado y comprender los orígenes de las masas de aire que contribuyen con partículas en la Estación Científica Antártica Peruana Machu Pichu (ECAMP), ubicada en la Isla Rey Jorge de la península Antártica. Se usaron colectores Partisol con filtros de teflón, perfilador contador de partículas y etalómetro. Los elementos químicos se analizaron por espectrometría de masas de plasma acoplada inductivamente (ICP-MS) y se aplicaron técnicas multivariadas y factor de enriquecimiento. Los elementos más abundantes en PM<sub>10</sub> y PM<sub>2.5</sub> fueron Na, Fe, Mg y Si, siendo las fuentes locales más importantes las de origen marino (Na, Mg, Mn, Ca) y de la corteza (Fe, Al, P). Se registraron también fuentes de meteorización (Ba y Si) propias del descongelamiento de los glaciares y fuentes de quema ligadas al uso de petróleo (V) y carbono negro. El estudio de las masas de aire sugiere una contribución potencialmente importante de fuentes externas. En general, se demuestra el impacto de fuentes antrópicas distantes y locales en el continente blanco.

### ABSTRACT

Antarctica is a remote and relatively pristine region, but the regional transport of aerosols may be a source of pollution, especially in the Antarctic Peninsula. Few studies have characterized atmospheric aerosols and evaluated the contribution of their emission sources. The Peruvian Antarctic research station Machu Pichu (ECAMP, by its Spanish acronym) is located on King George Island in the Antarctic Peninsula. During February 2020, atmospheric particulate mass (PM<sub>10</sub> and PM<sub>2.5</sub>) was sampled and analyzed to characterize its elemental composition and was supplemented by measurements of equivalent black carbon and aerosol size distributions. Chemical elements were analyzed by inductively coupled plasma mass spectrometry (ICP-MS), multivariate techniques, and enrichment factors. The most abundant elements in PM<sub>10</sub> and PM<sub>2.5</sub> were Na, Fe, Mg, and Si, with the most important local sources being marine (Na, Mg, Mn, Ca) and crustal (Fe, Al, P).

Sources of weathering (Ba and Si) from glacial thawing and sources of combustion linked to the use of oil (V) and emission of black carbon were recorded. Air mass back-trajectory analysis using the HYSPLIT model helped identify external sources of particulate matter in the air masses reaching the ECAMP site. Overall, this study supports the growing evidence of the anthropogenic impact of distant and local sources on the white continent.

**Keywords:** Antarctic, air mass trajectories, atmospheric aerosols, black carbon, particulate matter.

## 1. Introduction

Antarctica, known as the white continent, is a remote region interconnected with the rest of the world by oceanic and atmospheric couplings, which plays a dominant role in the climatic system. The thermohaline circulation, responsible for the large-scale heat transport in the Ocean, is deeply modulated in the Southern Hemisphere by the seasonal sea ice sheet formations in the Antarctic. The prevailing strong westerly winds surrounding the Antarctic near surface and the stratospheric polar vortex formed in spring are atmospheric patterns responsible for the oceanic Antarctic circumpolar current. These two examples alone underline the importance of the Antarctic for global climate. For these reasons, among others, there is an increasing historical interest in scientific research on the Antarctic region in addition to international geopolitical agreements. The fate of its ice sheets plays a dominant role in climate regulation (Luis, 2013; Kennicutt et al., 2019).

Antarctica is one of the most pristine and unexplored regions of the world. However, there is evidence that it is a sink for atmospheric aerosols transported from remote locations (Bargagli, 2016; Anzano et al., 2022), negatively affecting the ecosystems and environmental conditions of this continent (Marina-Montes et al., 2020). Depending on the wind and meteorological conditions, atmospheric aerosols can be transported thousands of kilometers in days (Zhong et al., 2019; Jia and Zhang, 2020; Xiong et al., 2020). This transport undergoes microphysical and chemical transformations, making it spatially and temporally non-uniform (Bellouin et al., 2020). Aerosol concentration, size distribution, chemical composition, and dynamic behavior in the atmosphere play a crucial role in governing radiative transfer and, thus, the climate system (Bellouin et al., 2020; Marina-Montes et al., 2020).

King George Island (KGI) is the largest of the South Shetland Islands. It is located on the Antarctic

Peninsula and contains many research stations (Polyakov et al., 2020). There are several reports about atmospheric aerosols conducted in the Antarctic Peninsula (Artaxo et al., 1992; Ángeles et al., 2020; Hong et al., 2020; Polyakov et al., 2020; Fan et al., 2021; Szumińska et al., 2021; Gonçalves et al., 2022). However, despite progress in characterizing and determining the origin of atmospheric aerosols (Marina-Montes et al., 2020), there is still limited information on the source areas of air masses that move particles toward the white continent.

The Peruvian Antarctic Scientific Station Machu Picchu (Estación Científica Antártica Machu Picchu, ECAMP) is located in the KGI, at the northern end of the Antarctic Peninsula, very close to the open ocean with maritime climatic conditions. ECAMP only operates during the Austral summer, covering periods from December to March at most (Ángeles et al., 2020), so studies on particles and their source areas at the site are still insufficient.

Therefore, this research aims to characterize the chemical composition of aerosol monitors and atmospheric particles at ECAMP, analyze the contribution of their emission sources, and investigate the origin of the air masses that contribute to their transport to the site during the austral summer of 2020. In this regard, this study provides the first valuable data set on trace elements and atmospheric particles in the understudied area of ECAMP. This dataset and reported results will contribute to filling a gap in the knowledge about aerosol behavior in ECAMP.

## 2. Materials and methods

### 2.1 Study site

The study site where the measurement and collection equipment were installed was the ECAMP (62.09° S, 58.47° W) in King George Island, north of the Antarctic Peninsula (Fig. 1). The sampling site was about 1 km east of the ECAMP's main building and about 20 m

from the sea coast. The mean annual temperature is  $-2.8\text{ }^{\circ}\text{C}$  with an annual precipitation of 729 mm. There are about 100 days of sunshine (Polyakov et al., 2020). The ECAMP is located south of Admiralty Bay (Mackellar Inlet) below the Machu Pichu Mountain, about 600 m from the Znosko Glacier. It has gravelly and sandy soils, with rocks and flood zones resulting from snow thawing.

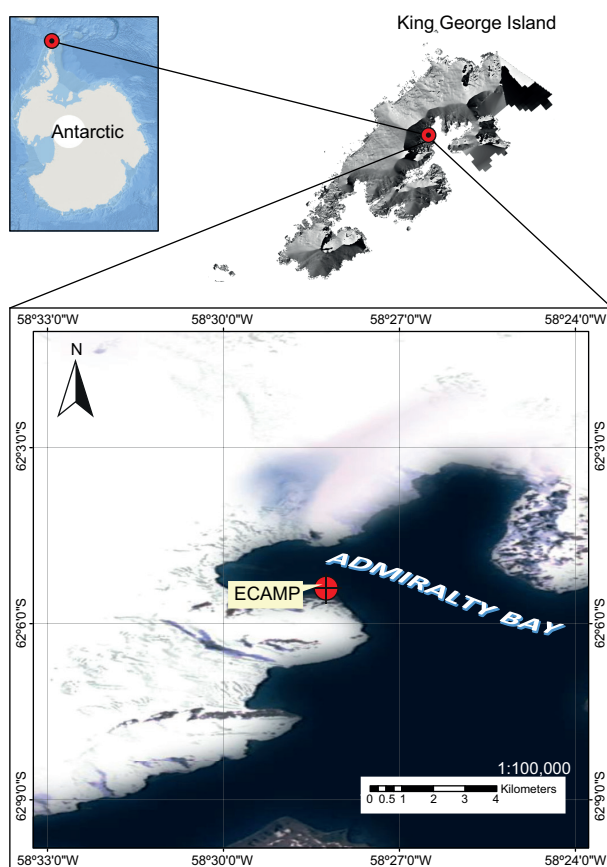


Fig. 1. Location of the sampling station in the Peruvian Scientific Station Machu Picchu (ECAMP) on King George Island, Admiralty Bay, Antarctic Peninsula ( $62.09^{\circ}\text{ S}$ ,  $58.47^{\circ}\text{ W}$ ).

## 2.2 Measurements

The sampling periods were between February 7 and 23, 2020, during the Peruvian Antarctic Campaign ANTAR XXVII organized by the Ministry of Foreign Affairs of Peru.  $\text{PM}_{2.5}$  and  $\text{PM}_{10}$  were collected simultaneously on a Teflon filter (diameter of 47 mm, pore size of  $2.0\text{ }\mu\text{m}$ , Whatman, USA) using two

Partisol samplers (model 2000-FRM, Thermo Scientific, USA). The first sampler was installed with a stainless steel  $2.5\text{ }\mu\text{m}$  cut point cyclone, and the other with an inlet-type sampling head to cut at  $10\text{ }\mu\text{m}$  (US-EPA). The flow rate was  $16.7\text{ L/min}$ . A total of five samples were collected (February 7-9, 10-13, 14-17, 17-20, and 20-23). The collection period was set at 72 h following the recommendation of Artaxo et al (1992), to ensure sufficient material was available for detecting trace elements in the filters. The filters with samples were stored and transported to the laboratory in Peru in labeled containers at  $4\text{ }^{\circ}\text{C}$ .

The sampling of atmospheric aerosols was complemented with aerosol size distribution measurements and black carbon (BC) concentration from February 4 to 23, 2020. The counting data were collected by a laser diode-based optical particle counter with eight channels (model 212, Met One Instruments, USA). The size channel ranges were  $0.3$ ;  $>0.3-0.5$ ;  $>0.5-0.7$ ;  $>0.7-1.0$ ;  $>1.0-2.0$ ;  $>2.0-3.0$ ;  $>3.0-5.0$ , and  $>5.0-10.0\text{ }\mu\text{m}$ . The channels will be named from now on the text as  $\text{PM}_{0.3}$ ,  $\text{PM}_{0.3-0.5}$ ,  $\text{PM}_{0.5-0.7}$ ,  $\text{PM}_{0.7-1}$ ,  $\text{PM}_{1-2}$ ,  $\text{PM}_{2-3}$ ,  $\text{PM}_{3-5}$ , and  $\text{PM}_{5-10}$ , respectively. The instruments continuously sampled air at  $1\text{ L/min}$  and provided data count per minute for each channel.

An Aethalometer (model AE33, Magee Scientific, USA) was used to measure the BC concentration. It is based on the change of absorbance of light through the pass of a filter continuously loaded with aerosols. The passing light is analyzed at seven wavelengths: 370, 470, 520, 590, 660, 880, and 950 nm. A  $2.5\text{ }\mu\text{m}$  cut point cyclone was placed at the inlet to avoid coarse particles. Particles in the incoming airflow are deposited on the polytetrafluoroethylene (PTFE) filter. The instrument operates continuously at a flow rate of  $5\text{ L/min}$  (Drinovec et al., 2015; Suárez et al., 2017).

The suction tubes of the installed instruments and Partisol samplers were mounted at 1 m from the ceiling level of the support platform and approximately 3 m above the ground level to avoid surface effects and soil contamination.

Meteorological data was obtained from the automatic meteorological station (Model Vaisala MAWS-301) installed at the Peruvian station by the Directorate of Aeronautical Meteorology of Peru (Dirección de Meteorología Aeronáutica, DIRMA)

during the study. This equipment was installed 4 m north of the sampling site.

### 2.3 Gravimetric analysis

PM<sub>10</sub> and PM<sub>2.5</sub> mass concentrations were determined by the gravimetric method using Teflon filters in the Partisol samplers. The filters were weighed before and after sampling using an electronic microbalance of ± 0.01 mg sensitivity (Mettler M3) in an environment with stable temperature and humidity, and the concentration was computed by dividing the weight gain of the filter by the volume of air sampled (Pfeiffer, 2005).

### 2.4 Chemical elemental determination in PM<sub>10</sub> and PM<sub>2.5</sub>

The inductively coupled plasma mass spectrometer (ICP-MS) technique determined the samples' elemental chemical composition. Filter samples were digested in a PTFE flask with 3 mL of HNO<sub>3</sub> (suprapure grade, Merck, Darmstadt) at 120 °C for 4 h on a hot plate. Then, the digested samples were diluted to 5% HNO<sub>3</sub>. The solution obtained was analyzed using an Elan DRC II ICP-MS (PerkinElmer SCIEX, USA). To correct instrumental drifts and plasma fluctuations, 103 Rh was used as an internal standard. Certified multi-element standards of trace elements were used to construct a six-point external calibration to quantify trace elements (Huamán et al., 2019). The following 33 trace elements were measured in the samples: Al, Sb, As, Ba, Be, Bi, B, Cd, Ca, Co, Cu, Cr, Sn, Sr, P, Fe, Li, Mg, Mn, Hg, Mo, Ni, Ag, Pb, K, Se, Si, Na, Ta, Ti, V, and Zn. The precision of the ICP-MS analysis was about 6% in the elements detected.

### 2.5 Data analysis

Descriptive statistics was used for concentrations of trace elements contained in aerosols, particle counting, and BC concentration for the entire campaign to characterize temporal behavior. Concentrations of trace elements of PM<sub>2.5</sub> and PM<sub>10</sub> samples were evaluated with Spearman's multiple correlation tests ( $p < 0.05$ ) to establish statistically significant dependencies.

The enrichment factor (EF) was calculated to study the influence of anthropogenic or natural activities on the measured chemical element. Titanium

was used as a crustal reference element for the EF, following the studies of Bazzano et al. (2015) and Marina-Montes et al. (2020). Calculation of the EF was performed according to Eq. (1) (Rahn, 1971):

$$EF = \frac{(X/T_i)_{air}}{(X/T_i)_{crustal}} \quad (1)$$

where  $X$  is the concentration of each trace element,  $X/T_i$  air is the concentration ratio between element  $X$  and the reference  $T_i$  element in the aerosol sample (PM<sub>2.5</sub> and PM<sub>10</sub>), and  $X/T_i$  crustal is the concentration ratio between the element  $X$  and the reference  $T_i$  element in the soil surrounding the sampling site, given its abundance (in ppm) in the Earth's crust (Wedepohl, 1995). Calculated EF values < 5 are explained as having a crustal or soil origin (Megido et al., 2017; Marina-Montes et al., 2020); if EF > 10 it indicates an enrichment attributable to additional sources, a significant fraction of anthropogenic origin (Chester et al., 2000; Bazzano et al., 2015; Marina-Montes et al., 2020).

Hierarchical cluster analysis (HCA) using Ward's method of linkage and the squared Euclidean distance for similarities was used to segregate associations within the group of trace elements to identify possible pollutant sources (Hastie et al., 2009). All statistical analyses were performed using the CRAN R free software, v. 3.3.2 (R Team Core, 2015), using the following R packages: factoextra (Kassambara and Mundt, 2016), ggplot2 (Wickham, 2016), cluster (Chavent et al., 2012; Maechler et al., 2015), and psych (Revelle., 2018).

To analyze the influence of air masses from distant areas on trace element variability, the Hybrid Lagrangian Single-Particle Integrated Trajectory (HY-SPLIT) model (Stein et al., 2015) from the National Oceanic and Atmospheric Administration (NOAA) Air Resources Laboratory (ARL) service was employed. The inverse trajectories (back-trajectories) were generated for 120 h (5 days backward) and 10 m above the ground. Meteorological reanalysis data from the Global Data Assimilation System (GDAS) with a horizontal resolution of 0.5° were used for running the model. Finally, the trajectories were grouped by chemical monitoring period and divided into eight different wind directions: north (N), northeast (NE),

east (E), southeast (SE), south (S), southwest (SW), west (W), and northwest (NW).

### 3. Results and discussions

#### 3.1 Chemical composition

Table I shows the average concentrations, standard deviation, and minimum and maximum values of the trace elements detected in PM<sub>2.5</sub> and PM<sub>10</sub> samples for the whole measurement period. For PM<sub>2.5</sub>, 12 elements were recorded, with the most abundant being, in decreasing order: Na > Si > Mg > Fe > Ca > Al; V (0.0012 µg m<sup>-3</sup>) and Cu (0.0013 µg m<sup>-3</sup>) were only detected once in the first and second sampling periods (February 7-9 and 10-13, respectively). In PM<sub>10</sub>, 16 trace elements were recorded, with the most abundant being, in decreasing order: Na > Fe > Si > Ca > Mg > Al. Other elements (As [0.0012 µg m<sup>-3</sup>], Hg [0.00015 µg m<sup>-3</sup>], Cu [0.0034 µg m<sup>-3</sup>], Pb [0.0021 µg m<sup>-3</sup>], and Zn [0.012 µg m<sup>-3</sup>]) were only detected once in the second sampling period.

PM<sub>10</sub> shows more significant variability compared to the PM<sub>2.5</sub>; likewise, the element with the greatest change in values in both particle sizes was Na. Considering the proportions of the elements detected in the PM<sub>2.5</sub>/PM<sub>10</sub> index, Na registered

43%, Al 47%, Mg 41%, Fe 21%, and Ca 20% in PM<sub>10</sub>, which indicates a dominance of these elements in the coarse fraction. The abundance of Na in PM<sub>10</sub> and PM<sub>2.5</sub> coincides with results obtained by Artaxo et al. (1992) at the Brazilian Antarctic Station Comandante Ferraz, the nearest scientific station to our study site.

#### 3.2 Enrichment factor

The enrichment factors determined during the chemical characterization sampling periods (Fig. 2) for PM<sub>2.5</sub> show values greater than 10 (indicating severe enrichment) for Mg, Na, P, and V. The behavior was similar in PM<sub>10</sub> for the first period, except for V, which was undetected. For the second period, the elements with EF values greater than 10 were Fe, Cu, and P in PM<sub>2.5</sub> and Mg, P, Na, As, Ca, Cu, Fe, Hg, Mn, Pb, and Zn in PM<sub>10</sub>. In the third period, only Na had a value higher than 10 in both particle sizes. Similarly, for the fourth period, Mg, Na, and P in PM<sub>2.5</sub> and Na in PM<sub>10</sub> showed values greater than 10. In the last period, Mg and Na had values greater than 10 in both particle sizes, and P exceeded 10 in PM<sub>10</sub>.

Hierarchical cluster analysis (HCA) was applied to the concentration of trace elements, revealing the existence of three distinct groups in both particle sizes

Table I. Statistical description of elements concentrations (average concentrations, standard deviation, maximum and minimum) for PM<sub>2.5</sub> and PM<sub>10</sub> samples during the whole campaign at the Antarctic Research Station Machu Picchu during the 2020 summer season.

Parameters	PM <sub>2.5</sub> (µg m <sup>-3</sup> )		Parameter	PM <sub>10</sub> (µg m <sup>-3</sup> )	
	Mean ± sd	Min-max		Mean ± sd	Min-max
PM <sub>2.5</sub> n = 5	4.04 ± 2.8	1.646-8.722	PM <sub>10</sub> n = 5	12.54 ± 8.72	4.591-25.721
Al n = 5	0.065 ± 0.07	0.00517-0.126	Al n = 5	0.141 ± 0.108	0.0172-0.280
Ba	nd		Ba n = 2	0.00179 ± 0.000151	0.00169-0.00190
Ca n = 5	0.068 ± 0.03	0.0363-0.127	Ca n = 3	0.340 ± 0.238	0.174-0.612
Fe n = 5	0.097 ± 0.12	0.00823-0.291	Fe n = 4	0.454 ± 0.362	0.0463-0.921
K n = 3	0.0127 ± 0.009	0.00641-0.0237	K	nd	nd
Mg n = 5	0.13 ± 0.09	0.0494-0.288	Mg n = 5	0.318 ± 0.17	0.135-0.545
Mn n = 2	0.00187 ± 0.0009	0.00122-0.00251	Mn n = 3	0.00632 ± 0.004	0.00280-0.0107
Na n = 5	0.933 ± 0.816	0.0352-2.24	Na n = 5	2.16 ± 0.854	1.17-3.24
P n = 3	0.0174 ± 0.00884	0.00720-0.0230	P n = 5	0.0246 ± 0.0232	0.00445-0.0621
Si n = 4	0.420 ± 0.23	0.208-0.815	Si n = 5	0.380 ± 0.07	0.291-0.455
Sr	Nd		Sr n = 3	0.0009 ± 0.0004	0.000494-0.00122
Ti n = 2	0.002 ± 0.0007	0.00148-0.00244	Ti n = 3	0.0046 ± 0.002	0.00240-0.00687

sd: standard deviation; n: number of samples where element was detected; min: minimum; max: maximum; nd: not detected

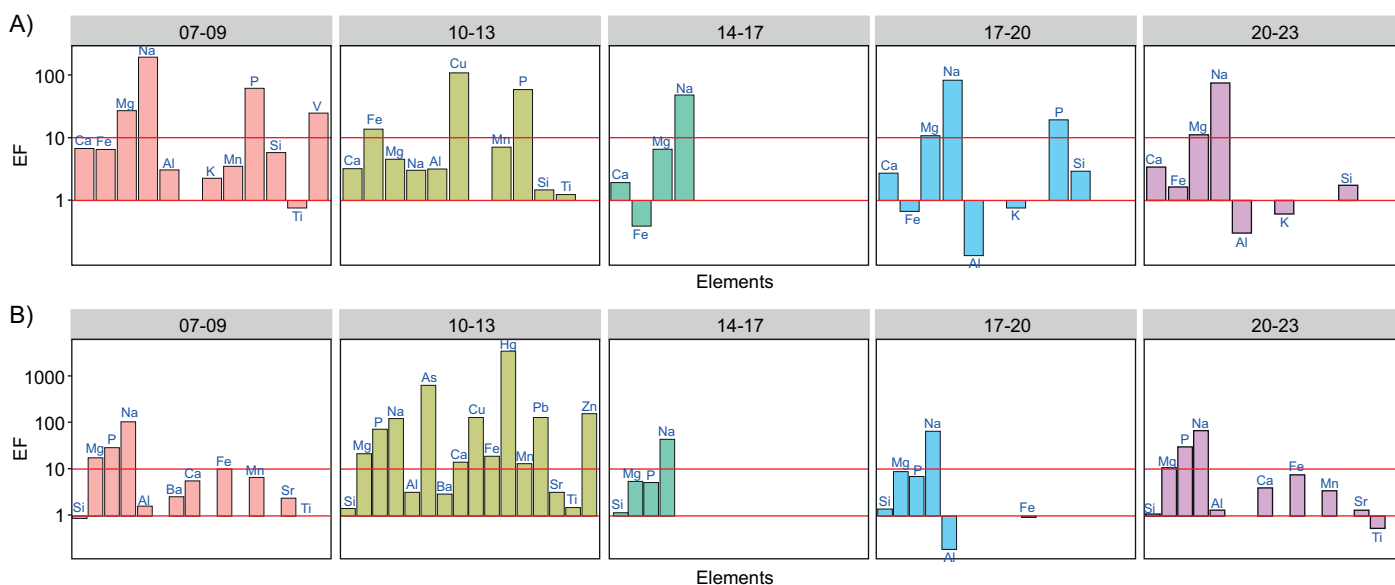


Fig. 2. Enrichment factors calculated for (a)  $PM_{2.5}$  and (b)  $PM_{10}$  for the chemical characterization sampling periods in the summer season of 2020 at the Antarctic Research Station Machu Picchu. Titanium was used as a reference (Wedepohl, 1995).

(Fig. 3). In the case of  $PM_{2.5}$ , Group I was formed by K, Si, Ca, Mg, and Na of marine origin. In contrast, Group II was formed by Ti and Mn, which are indicators of ocean sediments (Aquilina et al., 2014). Group III was formed by Fe, Al, and P, which generally have the Earth's crust as primary source. For  $PM_{10}$ , Group I was formed by Mg, Na, P, Al, and Fe. Group II was formed by Sr, Ti, Ca, and Mn, and Group III was formed by Ba and Si, indicating that Group I has its origin in marine for dominance of sea-salt elements, Group II in earth crust, and Group III in continental weathering, thus it may be used as an indicator of primary productivity and

meltwater input (Pyle et al., 2017). It should be noted that in both sizes, groupings of elements of marine and crustal origin have been identified as common sources, which aligns with the results of Artaxo et al. (1992).

### 3.3 Atmospheric particle size distribution

Increases in particles were observed on February 6, 10, 11, 16, 21, and 24, being more sustained from February 10 to 11, the days of the second chemical sampling period with the particle samplers (Fig. 4). Only in this period were recorded trace elements of anthropogenic origin such as As, Hg, Cu, Pb, and

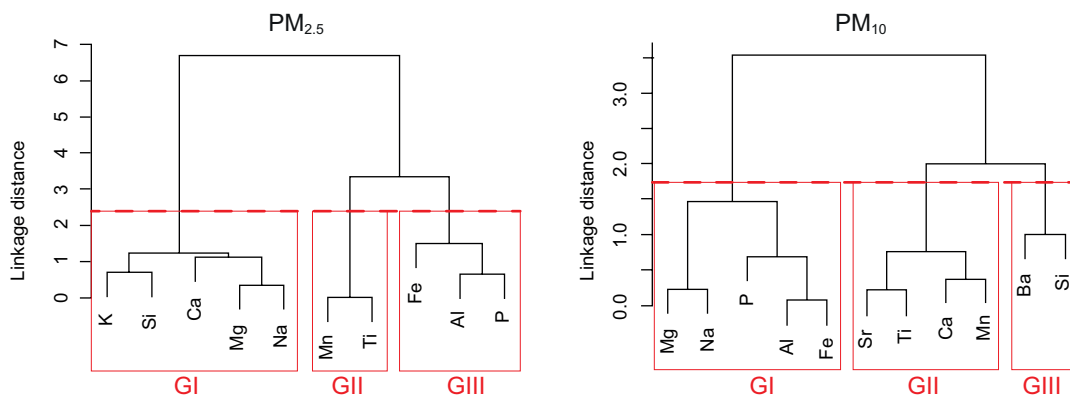


Fig. 3. Results of the hierarchical cluster analysis (dendrogram) of trace element concentrations measured in  $PM_{2.5}$  and  $PM_{10}$  during the 2020 summer season at the Antarctic Research Station Machu Picchu.

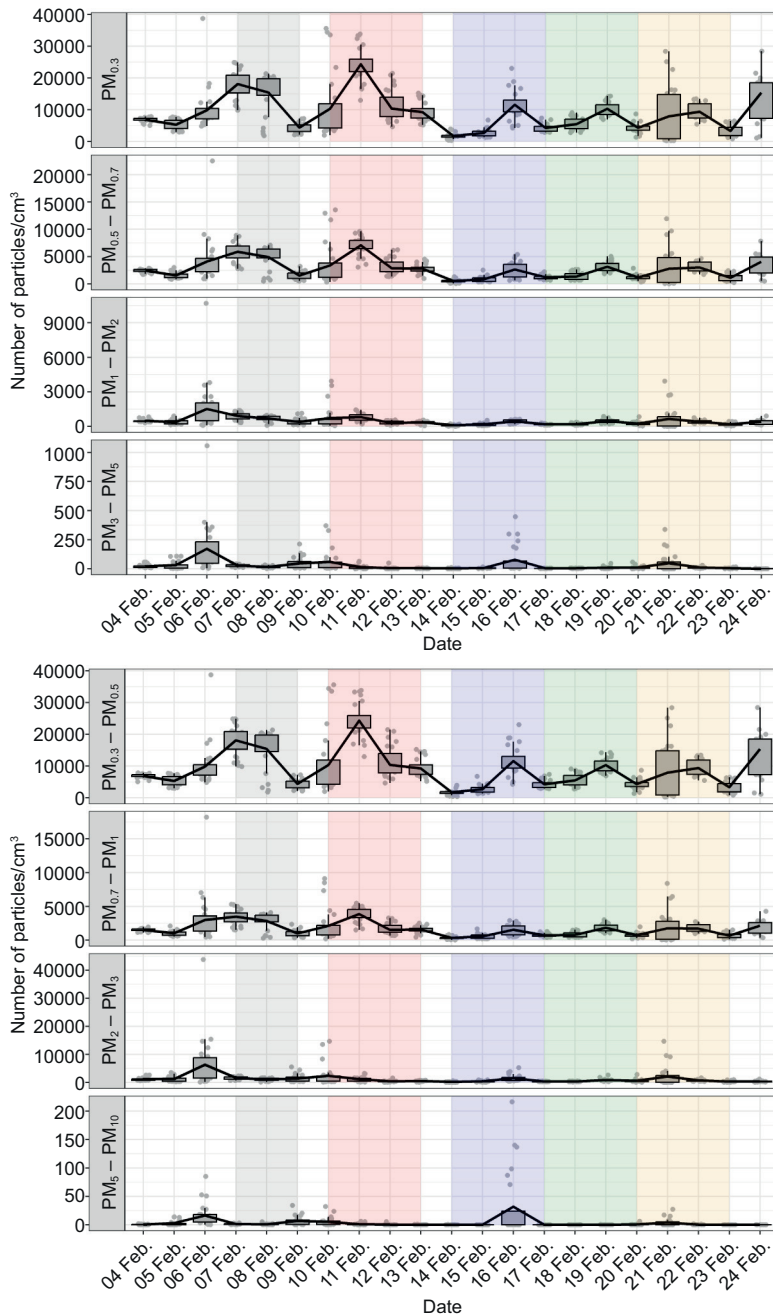


Fig. 4. Variation of atmospheric particle size distribution and concentration recorded for the whole monitoring period at the Antarctic Research Station Machu Picchu. The colored shadow bands represent the aerosol and chemical characterization sampling periods. (Gray: February 7-9; red: February 10-13; blue February 14-17; green: February 17-20; orange: February 20-23).

Zn. The colored shadow bands shown in Figure 4 represent the aerosol and chemical characterization sampling periods.

### 3.4 Black carbon

Increases in BC concentrations were observed on February 6, 9, 15, 21 and 24 (Fig. 5a), with the highest amount recorded on February 9, corresponding to the first chemical sampling period, with an apparent

sky, where the highest concentrations of Ca, K, Mg, Mn, Na, P, and Si were observed, in addition to the only record of V in  $PM_{2.5}$ , which would be related to activities linked to petroleum, together with fuel combustion processes at several research stations in the Antarctic subcontinent (John et al., 2023). On February 9 there were back trajectories of air masses that originated in the South American continent (Fig. 5b).

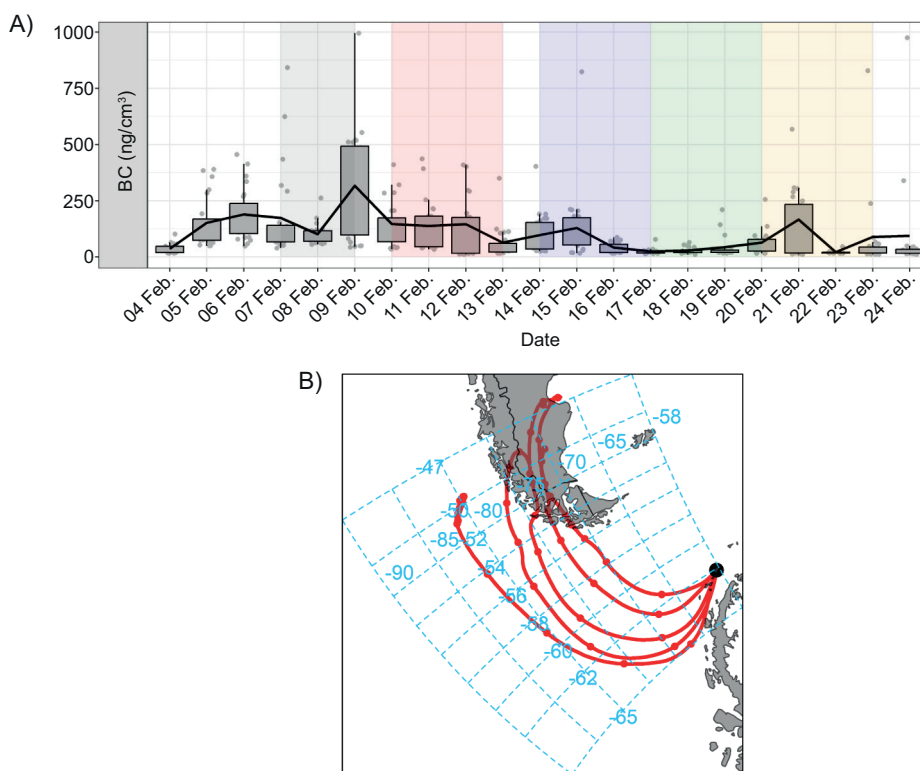


Fig. 5. (a) Variations in black carbon (BC) concentrations measured at the Antarctic Research Station Machu Picchu (ECAMP). The colored shadow band represents the sampling periods: gray: February 7-9; red: February 10-13; blue February 14-17; green: February 17-20; orange: February 20-23. (b) Air mass back trajectories calculated for February 9.

### 3.5 Trajectories

To investigate the possible origin of air masses contributing to the presence of aerosols over ECAMP during the studied period, a surface-level back trajectory analysis was conducted, separated by periods of chemical monitoring. The trajectories for each monitoring period were calculated with a 6-h interval and a backward duration of 120 h. Based on the obtained back trajectories (Fig. 6a), during the first monitoring period (February 7-9), the air masses originated from the South Pacific Ocean and the western side of the South American continent. In the second period (February 10-13), 25% of the air masses came from the South American continent, 50% from the Pacific Ocean, and the rest from the western Antarctic Ocean. In the third period (February 14-17), 73% of the air masses originated from the South American region, and 27% began in the

South Pacific Ocean and crossed the southern tip of the South American continent before reaching the study site. In contrast, during the fourth period (February 17-20), 94% of the air masses came from the east, from the South Atlantic Ocean and western South Atlantic Ocean, with only 5% showing continental South American influence. For the fifth period (February 20-23), the majority (93%) of the air masses came from the southern Pacific Ocean and 7% from the Atlantic Ocean, indicating variability in air mass behavior.

When analyzing the frequencies of back trajectories divided into eight wind directions (Fig. 6b), the west (W) direction was prevalent during the first, second, and fifth periods, with frequencies exceeding 50%, followed by the northwest (NW) direction. During the third and fourth periods, the frequencies of the east (E), north (N), and northeast

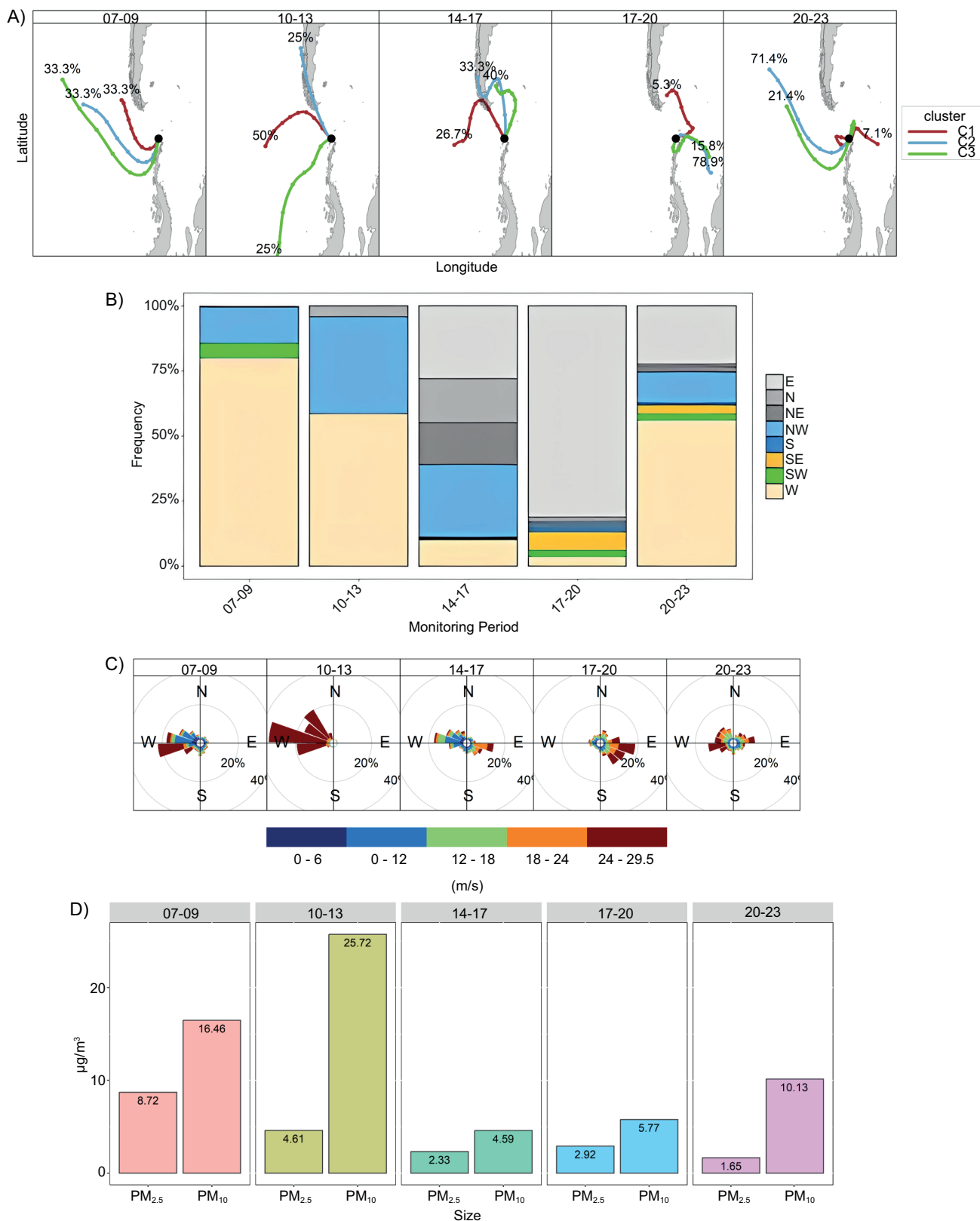


Fig. 6. (a) Air mass back trajectories (120 h backwards) at 10 m were calculated for each chemical monitoring period, and (b) frequency per chemical monitoring period of wind directions derived from the back-trajectory analysis. Eight directions were considered at the Antarctic Research Station Machu Picchu: north (N), northeast (NE), east (E), southeast (SE), south (S), southwest (SW), west (W), and northwest (NW) C) Wind roses obtained from the meteorological station installed at the Peruvian base by the Peruvian Aeronautical Meteorology Directorate during the study. (d) Mass concentration of PM<sub>10</sub> and PM<sub>2.5</sub> during the study.

(NE) directions increased, particularly noticeable in the third period, where the N direction had its highest frequency, coinciding with a higher inflow of air masses from the South American continent (more than 70%). In this period, Na showed an EF more significant than 10, indicating that the predominant sources were maritime.

When relating wind direction frequencies to PM<sub>10</sub> and PM<sub>2.5</sub> concentrations determined by filter collectors, PM<sub>2.5</sub> showed positive correlations with the southwest (SW) ( $r = 0.41$ ;  $p > 0.05$ ) and west (W) ( $r = 0.6$ ;  $p > 0.05$ ) directions and negative correlations with the N ( $r = -0.3$ ;  $p > 0.05$ ), E ( $r = -0.56$ ;  $p > 0.05$ ), NE ( $r = -0.88$ ;  $p > 0.05$ ), and south (S) ( $r = -0.45$ ;  $p > 0.05$ ) directions. For PM<sub>10</sub>, positive correlations were observed with the W ( $r = 0.8$ ;  $p > 0.05$ ) and NW ( $r = 0.3$ ;  $p > 0.05$ ) directions, and negative correlations with N ( $r = -0.4$ ;  $p > 0.05$ ), E ( $r = -0.88$ ;  $p > 0.05$ ), NE ( $r = -0.88$ ;  $p > 0.05$ ), and S ( $r = -0.34$ ;  $p > 0.05$ ) directions. This indicates that air masses from the W direction influence atmospheric particles, showing a stronger relationship with PM<sub>10</sub>. The W directions was more frequent in the first two periods of chemical sampling (Fig. 6c).

Correlating PM<sub>10</sub> and PM<sub>2.5</sub> concentrations with the most abundant elements in both particle sizes, Ca ( $r = 0.7$ ;  $p > 0.05$ ), Fe ( $r = 0.9$ ;  $p < 0.05$ ), Mg ( $r = 0.9$ ;  $p < 0.05$ ), and Na ( $r = 0.7$ ;  $p < 0.05$ ) showed the highest correlations with PM<sub>10</sub>. This suggests that the elements detected throughout the study period are primarily derived from coarse material, and local sources have more influence than remote ones. This information is supported by the results observed in the dendrograms, where they formed groups corresponding to sources of marine origin, crustal (soil), sedimentation, and rock weathering, as reported by Artaxo et al. (1992). In the study area, as in other places, the thawing of snow on glaciers has been occurring, releasing sedimentary rocks, gravels, and sands that, due to wind action, are carried and transported to other areas.

Figure 6c shows wind roses obtained from the meteorological station. During the first sampling monitoring period, the presence of V in PM<sub>2.5</sub> was recorded, which coincided with an increase in the concentrations of BC, being an indicator of sources related to the burning of fuel from the research stations and maritime transport. On February 9 tourist cruise ships were observed in the area, in addition to

trajectories of air masses originating in the south of the South American continent, which could indicate that there are remote sources of BC that can reach the study area.

In the second period, elements such as As, Hg, Cu, Pb, and Zn were detected in PM<sub>10</sub> corresponding to an EF greater than 10, which indicates their anthropogenic origin; when examining wind speeds, the highest wind speed and highest PM<sub>10</sub> concentration were recorded in the second period (Fig. 6d, suggesting that the elements with excessive enrichment were transported from nearby sources, being the ECAMP power generator (which operates with diesel fuel) the most likely source.

The results obtained in this study indicate that local sources, such as marine and crustal, are the main contributors to the studied atmospheric particles, which agrees with the findings published by Artaxo et al. (1992). An important aspect to consider is the sources of weathering, since with the retreat of glaciers the effect of wind erosion is an essential source in the area.

#### 4. Conclusions

Antarctica can be influenced by the transport of atmospheric PM from nearby and distant locations. It is crucial to characterize the particles to identify their sources, especially in the Antarctic Peninsula, which is closer to urban places in South America.

We were able to characterize the daily variation of particle size distribution in eight size ranges, where it was possible to note peaks related to aerosol transport.

Measurements of black carbon concentration indicated the influence of local combustion related to fossil fuel use from the scientific station.

The chemical characterization of PM<sub>10</sub> and PM<sub>2.5</sub> showed a predominance of elements related to marine origin, as expected from the area's characteristics. It also indicates the release of geological material that could contribute to the presence of elements such as Si, Ti, Al, and K in the PM.

There are external contributions (South America) and local contributions of black carbon such as burning, which, with the synergy of particles, could accelerate the melting of snow on the white continent.

## Acknowledgments

The authors would like to thank the Directorate of Antarctic Affairs of the Ministry of Foreign Affairs of the Peruvian Government and the Antarctic Operations Company of the Peruvian Army for their logistical support. Also, to the student Alfonso Torre Vitor for his work in the field during the campaign. Likewise, the authors acknowledge the support from internal research project PY-03-INV-18 of the University of Magallanes (UMAG).

## References

- Ángeles JM, Suárez L, Huaman AR, Ángeles R, Rosales G, Rocha A, Requena E, Muñoz F, Abi H. 2020. Direct radiative forcing due to aerosol properties at the Peruvian Antarctic station and Metropolitan Huancayo Area. *Anuário do Instituto de Geociências – UFRJ* 3: 404-412. [https://doi.org/10.11137/2020\\_4\\_404\\_412](https://doi.org/10.11137/2020_4_404_412)
- Anzano J, Abás E, Marina-Montes C, del Valle J, Galán-Madruga D, Laguna M, Cabredo S, Pérez-Arribas LV, Cáceres J, Anwar J. 2022. A review of atmospheric aerosols in Antarctica: From characterization to data processing. *Atmosphere* 13: 1-34. <https://doi.org/10.3390/atmos13101621>
- Aquilina A, Homoky WB, Hawkes JA, Lyons TW, Mills RA. 2014. Hydrothermal sediments are a source of water column Fe and Mn in the Bransfield Strait, Antarctica. *Geochimica et Cosmochimica Acta* 137: 64-80. <https://doi.org/10.1016/j.gca.2014.04.003>
- Artaxo P, Rabello ML, Maenhaut W, Grieken RV. 1992. Trace elements and individual particle analysis of atmospheric aerosols from the Antarctic peninsula. *Tellus B: Chemical and Physical Meteorology* 44: 318-334. <https://doi.org/10.3402/tellusb.v44i4.15460>
- Bargagli R. 2016. Atmospheric chemistry of mercury in Antarctica and the role of cryptogams to assess deposition patterns in coastal ice-free areas. *Chemosphere* 163: 202-208. <https://doi.org/10.1016/j.chemosphere.2016.08.007>
- Bazzano A, Soggia F, Grotti M. 2015. Source identification of atmospheric particle-bound metals at Terra Nova Bay, Antarctica. *Environmental Chemistry* 12: 245-252. <https://doi.org/10.1071/EN14185>
- Bellouin N, Quaas J, Gryspeerdt E, Kinne S, Stier P, Watson-Parris D, Boucher O, Carslaw KS, Christensen M, Daniau AL, Dufresne JL, Feingold G, Fiedler S, Forster P, Gettelman A, Haywood JM, Lohmann U, Malavelle F, Mauritsen T, McCoy DT, Myhre G, Mülmenstädt J, Neubauer D, Possner A, Rugenstein M, Sato Y, Schulz M, Schwartz SE, Sourdeval O, Storelvmo T, Toll V, Winker D, Stevens B. 2020. Bounding global aerosol radiative forcing of climate change. *Reviews of Geophysics* 58: 1-45. <https://doi.org/10.1029/2019RG000660>
- Chavent M, Kuentz-Simonet V, Lique B, Saracco J. 2012. ClustOfVar: An R package for the clustering of variables. *Journal of Statistical Software* 50: 1-16. <https://doi.org/10.18637/jss.v050.i13>
- Chester R, Nimmo M, Fones GR, Keyse S, Zhang Z. 2000. Trace metal chemistry of particulate aerosols from the UK mainland coastal rim of the NE Irish sea. *Atmospheric Environment* 34: 949-958. [https://doi.org/10.1016/S1352-2310\(99\)00234-4](https://doi.org/10.1016/S1352-2310(99)00234-4)
- Drinovec L, Močnik G, Zotter P, Prévôt ASH, Ruckstuhl C, Coz E, Rupakheti M, Sciare J, Müller T, Wiedensohler A, Hansen ADA. 2015. The "dual-spot" aethalometer: An improved measurement of aerosol black carbon with real-time loading compensation. *Atmospheric Measurement Techniques* 8, 1965-1979. <https://doi.org/10.5194/amt-8-1965-2015>
- Fan S, Gao Y, Sherrell RM, Yu S, Bu K. 2021. Concentrations, particle-size distributions, and dry deposition fluxes of aerosol trace elements over the Antarctic Peninsula in austral summer. *Atmospheric Chemistry and Physics* 21: 2105-2124. <https://doi.org/10.5194/acp-21-2105-2021>
- Gonçalves SJ, Magalhaes N, Charello RC, Evangelista H, Godoi RH. 2022. Relative contributions of fossil fuel and biomass burning sources to black carbon aerosol on the southern Atlantic Ocean coast and King George Island (Antarctic Peninsula). *Anais da Academia Brasileira de Ciências* 94: e20210805. <https://doi.org/10.1590/0001-376520220210805>
- Hastie T, Tibshirani R, Friedman J. 2009. *The elements of statistical learning: Data mining, inference and prediction*. Springer, New York.
- Hong SB, Yoon YJ, Becagli S, Gim Y, Chambers SD, Park KT, Park SJ, Traversi R, Severi M, Vitale V, Kim JH, Jang E, Crawford J, Griffiths AD. 2020. Seasonality of aerosol chemical composition at King Sejong Station (Antarctic Peninsula) in 2013. *Atmospheric Environment* 223: 117185. <https://doi.org/10.1016/j.atmosenv.2019.117185>
- Huamán A, Bendezu Y, Suárez-Salas L, Pomalaya J, Álvarez D, Gioda A. 2019. Chemical characterization

- of PM<sub>2.5</sub> at rural and urban sites around the metropolitan area of Huancayo (central Andes of Peru). *Atmosphere* 10: 1-17. <https://doi.org/10.3390/atmos10010021>
- Jia W, Zhang X. 2020. The role of the planetary boundary layer parameterization schemes on the meteorological and aerosol pollution simulations: A review. *Atmospheric Research* 239: 104890. <https://doi.org/10.1016/j.atmosres.2020.104890>
- John PM, Sanjeevan VN, Gopinath A. 2023. Distribution of vanadium in the surficial sediments of Prydz Bay, Indian sector of the Southern Ocean. *Soil and Sediment Contamination: An International Journal* 32: 363-375. <https://doi.org/10.1080/15320383.2022.2090501>
- Kassambara A, Mundt F. 2016. Extract and visualize the results of multivariate data analyses. R Package. Available at <https://rpkgs.datanovia.com/factoextra/index.html> (accessed 2022 April 25)
- Kennicutt MC, Bromwich D, Liggett D, Njåstad B, Peck L, Rintoul SR, Ritz C, Siegert M, Aitken A, Brooks C, Cassano J, Chaturvedi S, Chen D, Dodds K, Golledge N, Bohec C, Leppe M, Murray A, Nath P, Raphael M, Rogan-Finnemore M, Schroeder D, Talley L, Travouillon T, Vaughan D, Wang L, Weatherwax A, Yang H, Chown SL. 2019. Sustained Antarctic research: A 21st century imperative. *One Earth* 1: 95-113. <https://doi.org/10.1016/j.oneear.2019.08.014>
- Luis AJ. 2013. Past, present and future climate of Antarctica. *International Journal of Geosciences* 4: 959-977. <http://doi.org/10.4236/ijg.2013.46089>
- Maechler M, Rousseeuw P, Struyf A, Hubert M, Hornik K, Studer M, Roudier P. 2015. Finding groups in data: Cluster analysis extended Rousseeuw. Available at <https://cran.r-project.org/web/packages/cluster/index.html> (accessed 2022 October 22)
- Marina-Montes C, Pérez-Arribas LV, Escudero M, Anzano J, Cáceres JO. 2020. Heavy metal transport and evolution of atmospheric aerosols in the Antarctic region. *Science of The Total Environment* 721: 137702. <https://doi.org/10.1016/j.scitotenv.2020.137702>
- Megido L, Negral L, Castrillón L, Suárez-Peña B, Fernández-Nava Y, Marañón E. 2017. Enrichment factors to assess the anthropogenic influence on PM<sub>10</sub> in Gijón (Spain). *Environmental Science and Pollution Research* 24: 711-724. <https://doi.org/10.1007/s11356-016-7858-8>
- Pfeiffer RL. 2005. Sampling for PM<sub>10</sub> and PM<sub>2.5</sub> particulates. *Micrometeorology in Agricultural Systems* 47: 227-245. <https://doi.org/10.2134/agronmonogr47.c11>
- Polyakov V, Abakumov E, Mavlyudov B. 2020. Black carbon as a source of trace elements and nutrients in ice sheet of King George Island, Antarctica. *Geosciences* 10: 465. <https://doi.org/10.3390/geosciences10110465>
- Pyle KM, Hendry KR, Sherrell RM, Meredith MP, Venables H, Lagerström M, Morte-Rodenas A. 2017. Coastal barium cycling at the west Antarctic Peninsula. *Deep Sea Research Part II: Topical Studies in Oceanography* 139: 120-131. <https://doi.org/10.1016/j.dsr2.2016.11.010>
- R Team Core. 2015. A language and environment for statistical computing. R Foundation for Statistical Computing, Vienna.
- Rahn KA. 1971. Sources of trace elements in aerosols: An approach to clean air. Department of Meteorology and Oceanography, The University of Michigan. Available at <https://deepblue.lib.umich.edu/handle/2027.42/7201> (accessed 2020 June 2)
- Revelle W. 2018. Procedures for psychological, psychometric, and personality research. Available at <https://cran.r-project.org/web/packages/psych/index.html> (accessed 2020 November 14)
- Stein AF, Draxler RR, Rolph GD, Stunder BJB, Cohen MD, Ngan F. 2015. NOAA's HYSPLIT atmospheric transport and dispersion modeling system. *Bulletin of the American Meteorological Society* 96: 2059-2077. <https://doi.org/10.1175/BAMS-D-14-00110.1>
- Suárez L., Torres C, Helmig D, Hueber J. 2017. Medición y análisis del aerosol de carbono negro en el observatorio de Huancayo, Perú. *Revista Boliviana de Física* 30: 9-17.
- Szumińska D, Potapowicz J, Szopińska M, Czapiewski S, Falk U, Frankowski M, Polkowska Ż. 2021. Sources and composition of chemical pollution in Maritime Antarctica (King George Island). Part 2: Organic and inorganic chemicals in snow cover at the Warszawa Icefield. *Science of The Total Environment* 796: 149054. <https://doi.org/10.1016/j.scitotenv.2021.149054>
- Wedepohl KH. 1995. The composition of the continental crust. *Geochimica et Cosmochimica Acta* 59: 1217-1232. [https://doi.org/10.1016/0016-7037\(95\)00038-2](https://doi.org/10.1016/0016-7037(95)00038-2)
- Wickham H. 2016. *ggplot2: Elegant graphics for Data analysis*. Springer, New York. Available at <https://cran.r-project.org/web/packages/ggplot2/index.html> (accessed 2023 October 23).
- Xiong J, Zhao T, Bai Y, Liu Y, Han Y, Guo C. 2020. Climate characteristics of dust aerosol and its transport in major global dust source regions. *Journal of Atmospheric*

and Solar-Terrestrial Physics 209: 105415. <https://doi.org/10.1016/j.jastp.2020.105415>

Zhong J, Zhang X, Wang Y, Wang J, Shen X, Zhang H, Wang T, Xie Z, Liu C, Zhang H, Zhao T, Sun J, Fan S, Gao Z, Li Y, Wang L. 2019. The two-way feedback

mechanism between unfavorable meteorological conditions and cumulative aerosol pollution in various haze regions of China. *Atmospheric Chemistry and Physics* 19: 3287-3306. <https://doi.org/10.5194/acp-19-3287-2019>